Applied Physics B (2023) 129:160
https://doi.org/10.1007/s00340-023-08103-x

Applied Physics B
Lasers and Optics

RESEARCH

Single-crystal and ceramic Yb:Lu_2O_3 gain media for thin-disk oscillators

Stefan Esser[1] · Xiaodong Xu[2] · Jun Wang[2] · Jian Zhang[3] · Thomas Graf[1] · Marwan Abdou Ahmed[1]

Received: 3 August 2023 / Accepted: 8 September 2023 / Published online: 27 September 2023
© The Author(s) 2023

Abstract
We report on the direct comparison of single-crystal and ceramic Yb^{3+}:Lu_20_3 gain media with respect to emission spectra, fluorescence lifetime, depolarization, and laser performance in a continuous-wave thin-disk laser oscillator. The most efficient laser operation was achieved with a single-crystal disk in multimode operation with a slope efficiency of 72.1% and an average output power of 997 W. At the same temperature level, a ceramic disk delivered 861 W with a slope efficiency of 68.6%. In fundamental-mode operation, the highest average power of 360 W and highest optical efficiency of 41.3% were obtained with a ceramic disk. For the single-crystal disk, the fundamental-mode output power was limited to 113 W at an optical efficiency of 29%, potentially due to stress within the crystal.

1 Introduction

The sesquioxide crystal Yb^{3+}:Lu_2O_3 is a gain medium with excellent potential for thin-disk lasers operating at high average powers. Efficient pumping is possible thanks to its narrow but high absorption peak with an absorption cross-section of $\sigma_{abs} = 3.1 \cdot 10^{-20}$ cm^2 at a wavelength of 976 nm [1]. The quantum defect amounts to only 5.6% with a laser emission centered at 1034 nm [2]. In addition to the low heat generation, the thermal conductivity of Yb:Lu_2O_3 amounts to 12 W/mK, which is almost twice the value of the heat conductivity of the well-established laser crystal Yb:YAG (both at the same Yb-ion density of $8 \cdot 10^{20}$ cm^{-3}) [1]. Additionally, Yb:Lu_2O_3 exhibits a comparatively broad emission bandwidth of 13 nm full width at half maximum (FWHM) [3] which is especially interesting for mode-locking to obtain pulse durations in the order of 100 fs and below.

Yet, the high melting point of 2450 °C [2] is a challenge for the growth of Yb:Lu_2O_3 single crystals. Thus, the availability of high-quality single crystals with sizes exceeding about 10 mm is very limited. Larger laser-grade Yb:Lu_2O_3 samples can be produced by means of ceramic manufacturing techniques as shown in [4], where the sintering temperatures are significantly lower with maximum at 1700 °C.

When comparing the record thin-disk laser results for ceramic and single crystalline Yb:Lu_2O_3, the highest overall slope efficiency of 85% was attained with a single crystal together with an output power of 301 W [1]. The highest slope efficiency achieved with a ceramic Yb:Lu_2O_3 disk was 74% with a maximum output power of 16 W [5]. The highest ever-published output power of 1.19 kW from a Yb:Lu_2O_3 laser so far was achieved with a ceramic disk and the slope efficiency amounted to 65% [6]. The highest output power published for a single-crystal Yb:Lu_2O_3 disk is 670 W and the corresponding slope was 80% [7]. These cited publications are all devoted to either the ceramic or the single-crystal disks which impedes a detailed comparison.

We, therefore, report on a comparative study of single-crystal and poly-crystalline ceramic Yb:Lu_2O_3 gain media with regard to their emission spectra, fluorescence lifetime, depolarization, and laser performance in a continuous- wave (cw) multimode (MM) and fundamental transverse-mode (FM) thin-disk oscillator.

✉ Stefan Esser
stefan.esser@ifsw.uni-stuttgart.de

[1] Institut Für Strahlwerkzeuge (IFSW), University of Stuttgart, Pfaffenwaldring 43, 70569 Stuttgart, Germany

[2] Jiangsu Key Laboratory of Advanced Laser Materials and Devices, School of Physics and Electronic Engineering, Jiangsu Normal University, Xuzhou 221116, China

[3] Key Laboratory of Transparent and Opto-Functional Inorganic Materials, Shanghai Institute of Ceramics, Chinese Academy of Science, Shanghai 201899, China

2 Disk characterization

2.1 Materials

Three different Yb^{3+}-doped Lu_2O_3 disks were investigated—a 3 at.% Yb:Lu_2O_3 single-crystal disk (referred to as "*SC 3%*" in the following), a 4 at.%- and a 5 at.% Yb:Lu_2O_3 poly-crystalline ceramic disk (referred to as "*PC 4%*" and "*PC 5%*", respectively). Photographs of the three samples are shown in Fig. 1. The disk *SC 3%* was grown using the heat-exchanger method at the ILP Hamburg [8] and was polished to a thickness of 115 µm. The two ceramic samples were fabricated by the Jiangsu Normal University in Xuzhou, using a combination of vacuum sintering and hot isostatic pressing of high-purity powders, similar to the approach described in [4]. The thickness of the disk *PC 4%* was 125 µm and that of disk *PC 5%* was 100 µm. The grain size of the ceramics ranged from 5 µm to 40 µm and both samples were free of pores. All three disks had a diameter of 11 mm and were anti-reflection (AR) coated at their front face and highly reflective (HR) at their rear face for both the pump and the laser wavelengths. Each disk was glued on a water-cooled diamond heat sink for efficient heat removal.

2.2 Emission spectra

The emission spectra were measured by exciting the disks with a cw diode laser with a spectrum centered at a wavelength of 976.5 nm and a spectral width of 0.4 nm FWHM. The diode laser was focused on the disks with a spot size of 5.5 mm under an angle of 32° and a power density of 21 W/cm^2. The emission spectra were recorded by a spectrometer covering the wavelength range between 900 and 1100 nm, coupled with a multimode fiber facing under an angle of 0° toward the disks.

The peak-normalized emission spectra shown in Fig. 2 exhibit no significant difference between the three samples. The emission peaks of all the three samples are centered at a wavelength of 1033 nm.

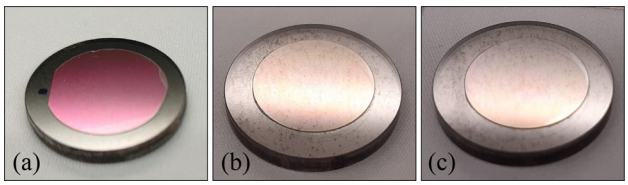

Fig. 1 Yb:Lu_2O_3 thin disks glued on diamond heat sinks: **a** disk SC 3%, **b** disk PC 4%, **c** disk PC 5%

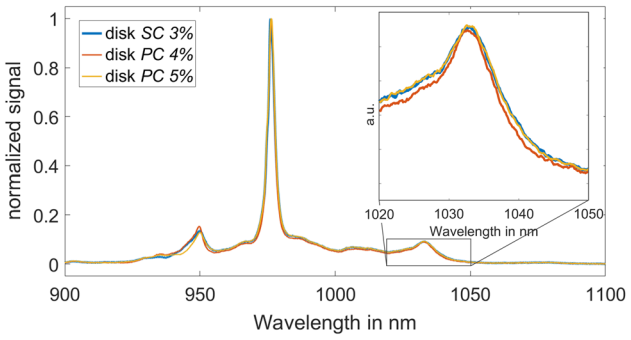

Fig. 2 Peak-normalized cw emission spectra of the three Yb:Lu_2O_3 samples recorded during excitation at a wavelength of 976.5 nm

2.3 Fluorescence lifetime

The fluorescence lifetime was measured immediately after turning off the excitation (falltime < 5 µs) using a spectral filter (transmission wavelength 1020 nm–1040 nm) and an ultrafast photodiode (falltime < 50 ps). The resulting decay curves are shown in Fig. 3.

The fluorescence lifetimes were measured to amount to 988 µs for disk *SC 3%*, 914 µs for disk *PC 4%,* and 903 µs for disk *PC 5%*. The lifetime measured for the single crystal *SC 3%* is close to the value of 975 µs previously reported for single-crystal Yb:Lu_2O_3 [8]. The lifetimes of the ceramic samples are about 8% shorter than the one of the single-crystal sample but significantly longer than the values previously reported for Yb:Lu_2O_3 ceramics, of 750 µs [5] and 710 µs [9]. This indicates an improved purity of the present ceramic samples.

Nevertheless, the shortened lifetimes of both ceramics in comparison to the single-crystal sample indicate the presence of quenching of the dopant's upper states and parasitic processes within the ceramic samples. The shortened lifetimes may be associated with higher losses during laser

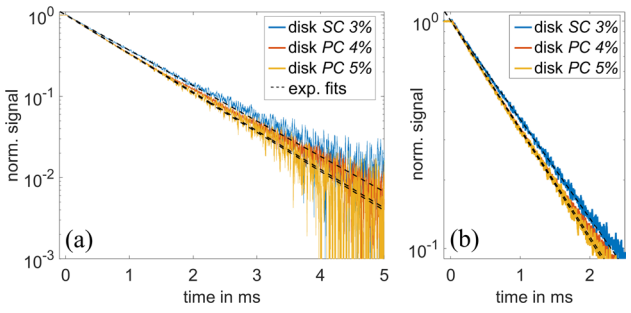

Fig. 3 Measured fluorescence decay and exponential fits (black dashed): **a** decay during the first 5 ms after turning off the excitation. **b** Excerpt showing the first 2 ms

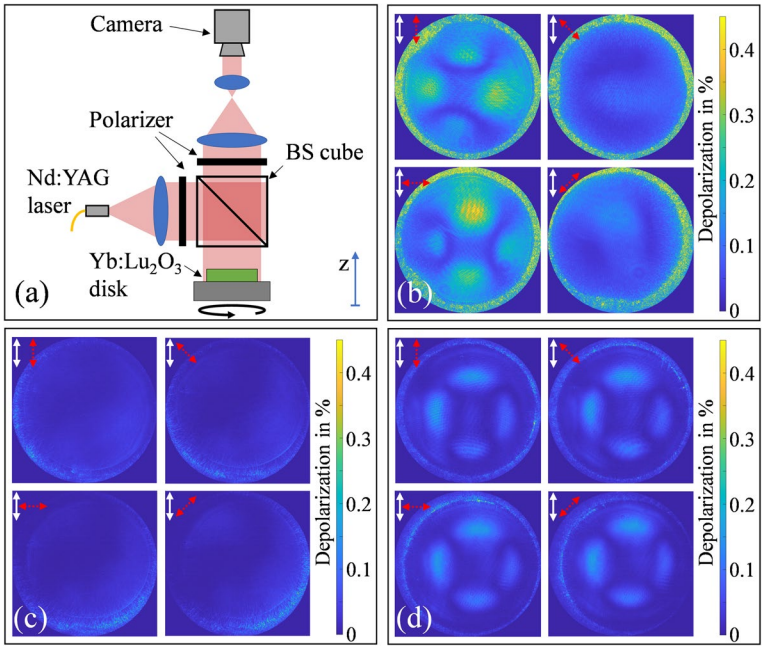

Fig. 4 **a** Crossed-polarizer arrangement to measure the depolarization. The cube beam splitter (BS) is non-polarizing. **d** Depolarization images of the three Yb:Lu_2O_3 disks. **b** disk *SC 3%*, **c** disk *PC 4%*, **d** disk *PC 5%*

operation which is consistent with higher resonator losses measured for the ceramics, as will be shown in Sect. 3.1 (see Fig. 6).

2.4 Depolarization images

To assess the presence of stress [10] within the otherwise isotropic material [3], the depolarization of the disks was measured by illuminating the samples at normal incidence with a Nd:YAG laser beam with a power of 44 mW at a wavelength of 1064 nm in a crossed-polarizers arrangement as depicted in Fig. 4a. The signal of the camera was calibrated with the two polarizers set to a parallel orientation (100% transmittance) and using a highly reflective mirror and a calibrated attenuation filter to replace the Yb:Lu_2O_3 disk.

The depolarization images of the three different disks are shown in Fig. 4b, c, and d. For each sample, four images were taken with the disks rotated by 0°, 45°, 90°, and 135° around the z-axis, with respect to an arbitrarily chosen initial angle of 0°. The white arrows in Fig. 4b–d represent the orientation of the input polarization, and the red-dashed arrows show the relative orientation of the disks with respect to their initial orientation.

The highest average amount of depolarization of 0.081% was observed for the disk *SC 3%*. The lowest average depolarization of 0.013% was found for the disk *PC 4%*. The one of the disk *PC 5%* was measured to be 0.03%.

The spatial distribution of the depolarization observed in the cross-sectional area of the disk *PC 5%* is typical for a radially symmetric stress distribution [11] and may be the

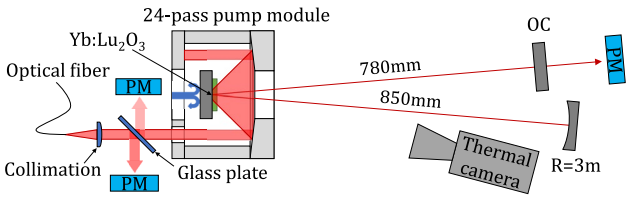

Fig. 5 Setup for MM operation: Yb:Lu_2O_3 disk (green) mounted on a water-cooled diamond heat sink, multi-pass pump module, and V-shaped laser cavity. For the sake of clarity, the drawing of the pump module does neither show all optical components nor the individual bam paths. Power meters (PM) are depicted in blue

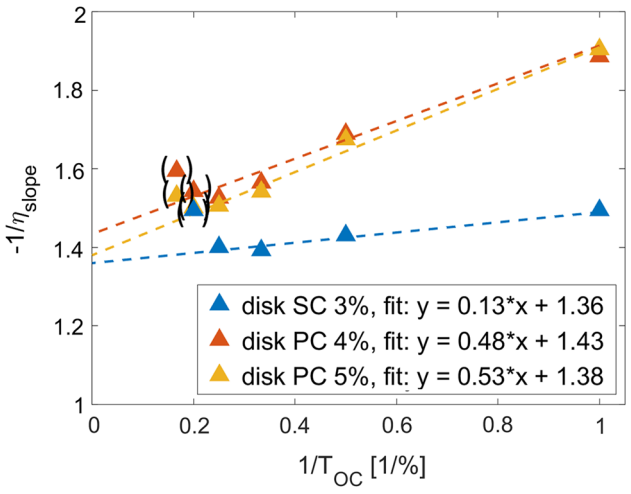

Fig. 6 Caird analysis of the Yb:Lu_2O_3 disks in continuous-wave multimode operation. The linear fits are applied to the data points without a bracket

result of an inhomogeneous pressure distribution during sintering.

The dependence of the depolarization on the orientation of the disk exhibited by the sample *SC 3%* indicates a correspondingly asymmetric distribution of the stress in the single crystal, which may be caused by asymmetric crystallization conditions during the growth.

Disk *PC 4%* shows a uniform distribution of depolarization. Hence, this disk is the most suitable one for laser operation where polarization preservation is of importance.

3 Laser experiments

3.1 Multimode operation

The three different Yb:Lu_2O_3 gain media were first operated in a cw MM thin-disk oscillator, with the experimental setup shown in Fig. 5. Each disk was mounted inside a multi-pass pump module that allows for 24 passes of the pump light through the crystal (12 reflections at the rear side of the disk). The diameter of the pump spot on the disk was set to 5.5 mm. A spectrally stabilized fiber-coupled diode laser with an output power of 2 kW and a 0.4 nm wide emission spectrum (FWHM) centered at a wavelength of 976.5 nm was used for pumping. The absorption of the pump light after 24 passes through the disk was measured by inserting a thin uncoated glass plate at an angle of 45° into the beam path outside the pump module (see Fig. 5). The absorption at each maximum pump power was 91% for disk *SC 3%* and 96.5% for disk *PC 4%* and *PC 5%*, respectively. The surface temperature of the disk was recorded with a thermal camera.

The V-shaped MM cavity was formed by a concave HR end mirror (radius of curvature RoC = 3 m), the disks (RoC = 3.8 m) and a plane output coupler (OC). This cavity generated a laser beam with a beam propagation factor of $M^2 = 15$. The wavelength of the laser emission was centered at 1033 nm in all experiments.

First, the resonator losses are measured after Caird et al. [12], by varying the transmission of the OCs and plotting the inverse slope efficiency against the inverse transmission rate, as shown in Fig. 6. A linear fit is applied to the data points and its slope corresponds to the resonator losses. Losses due to non-perfect coatings are estimated to be around 0.05% in this cavity; hence, the measured resonator loss is mainly a loss due to the Yb:Lu_2O_3 disks.

The lowest resonator losses are measured for disk *SC 3%* with 0.13%. For the ceramic disks, the resonator losses are significantly higher with 0.48% for disk *PC 4%* and 0.53% for disk *PC 5%*. This is consistent with the shortened lifetime of the ceramics which indicates parasitic loss processes. Additionally, we suspect scattering at the grain boundaries to contribute to the higher losses for the ceramics.

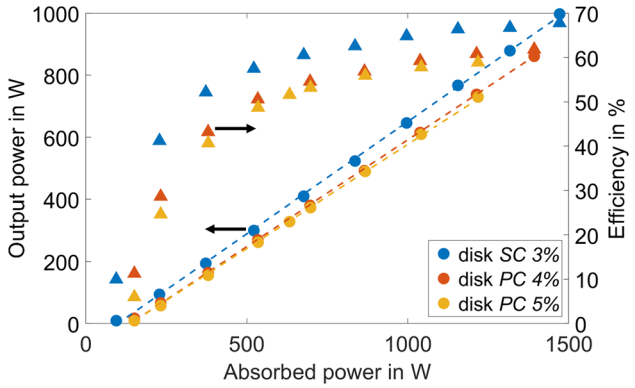

Fig. 7 Output power (circles), linear fit (dashed line), and optical efficiency (triangles) versus absorbed pump power in cw MM operation

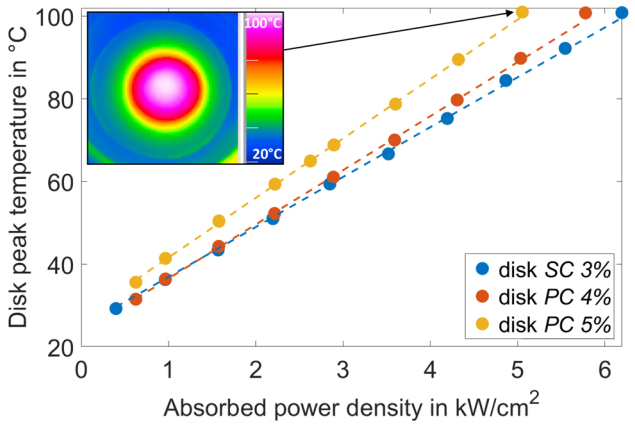

Fig. 8 Maximum surface temperature on the disks versus absorbed power density. Linear interpolations (dashed lines) were fitted to the data points. The inset exemplarily shows the thermal image of disk *PC 5%*

Furthermore, the Caird analysis gives the OC transmission with the highest slope efficiency which is found to be 3% for disk *SC 3%*, and 4% for the disks *PC 4%* and *PC 5%*.

The high-power MM laser test was conducted with the respective optimum OCs. The output powers and optical efficiencies are shown in Fig. 7 as a function of the absorbed pump power. The corresponding peak surface temperatures on the laser disks during MM operation are shown in Fig. 8 as a function of the absorbed power density. To minimize the risk of a thermally-induced damage, each disk was pumped up to a maximum surface temperature of 100 °C (see Fig. 8).

The highest slope efficiency of 72.1% and the highest output power of 997 W were obtained with the disk *SC 3%*.

An output power of 861 W with a slope efficiency of 68.6% was reached with the disk *PC 4%*. The disk *PC 5%* delivered an output power of 729 W with a slope efficiency of 66.9%.

It is assumed that residual losses within the ceramic disks are the main reason for the slightly reduced slope efficiencies compared to disk *SC 3%*.

Yet it is to be noted, that all disks do not exploit the maximum possible slope efficiency, which would only be limited by the quantum defect, and hence amount to 94.5%. Thus, there are still loss mechanisms that reduce the maximum achievable slope efficiency and that are not yet fully understood.

The lowest temperature rise was observed with the disk *SC 3%* with a slope of 12.4 K/(kW/cm^2), followed by disk *PC 4%* with a slope of 13.1 K/(kW/cm^2) and disk *PC 5%* with a slope of 14.4 K/(kW/cm^2).

A correlation between the temperature rise and the laser efficiency can be observed. Disk *SC 3%* showed the lowest temperature rise and at the same time the highest slope efficiency during MM laser operation. The lowest slope efficiency and the highest temperature rise were found with disk *PC 5%*. In fact, a lower efficiency in laser operation means that a lower fraction of the absorbed pump power is extracted out of the gain medium. Thus, more energy can be converted into heat.

Also, the ceramics shortened lifetime and relatively high resonator losses are consistent with their increased temperature rise, since both indicate the presence of non-radiative transitions of excited ions which would also contribute to the heating.

3.2 Fundamental-mode operation

A sketch of the setup used for fundamental-mode operation is shown in Fig. 9. The cavity consisted of a plane OC, the laser disk, two plane HR folding mirrors, and a concave HR end mirror with a radius of curvature of 1 m. The same output coupling as for the MM operation was used, i.e., 3% for disk *SC 3%* and 4% for disk *PC 4%* and disk *PC 5%*. The end mirror was placed on a linear stage to fine-tune the ratio between the diameter of the laser mode and the diameter of the pump spot by adapting the mirror's axial position.

The output power and optical efficiency obtained in fundamental-mode operation are shown in Fig. 10 as a function of the absorbed pump power.

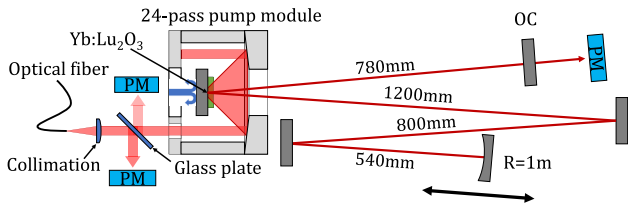

Fig. 9 Setup for fundamental-mode operation. For the sake of clarity, the drawing of the pump module does neither show all optical components nor the individual bam paths

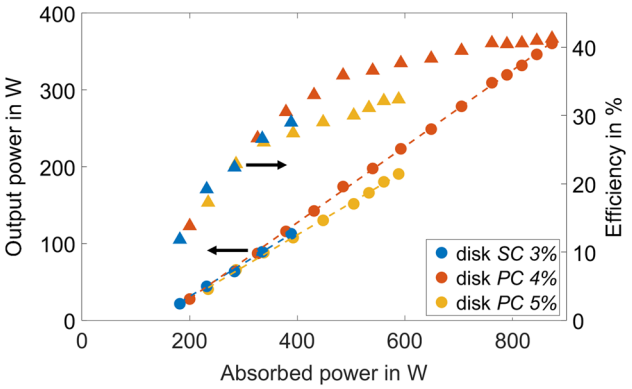

Fig. 10 Output power (circles), linear fit (dashed line), and optical efficiency (triangles) versus absorbed pump power in cw FM operation

The corresponding M^2 values are shown in Fig. 11 as a function of the laser output power. With a nominal ratio between the diameter of the fundamental mode and the diameter of the pump spot of 0.8, the M^2 values were kept below 1.2 across the entire power range for all three disks.

The highest output power of 360 W together with a slope efficiency of 49.6%, an optical efficiency of 41.3%, and $M^2 = 1.1$ was achieved with disk *PC 4%*. An output power of 190 W and $M^2 = 1.1$ was achieved with disk *PC 5%*, with a slope efficiency of 41.6% and an optical efficiency of 32.4%.

For both ceramic disks, further power increase was limited due to thermal lensing, by reaching the stability limits of the fundamental-mode resonator. The thermal lens was measured during fundamental-mode operation by means of a UV interferometer. It amounted to −89 mdpt/kW for disk *PC 5%* and to −39 mpdt/kW for disk *PC 4%*. Consequently, the power limitation of this cavity was reached at a lower power with disk *PC 5%*. Note that the negative sign of the thermal lenses arise from the fact that the cross-sectional temperature distribution shows a dip in the center during fundamental-mode operation due to the Gaussian-shaped extraction. Together with a positive *dn/dT* and *dl/dT* [13], this leads to a negative thermal lens in our case.

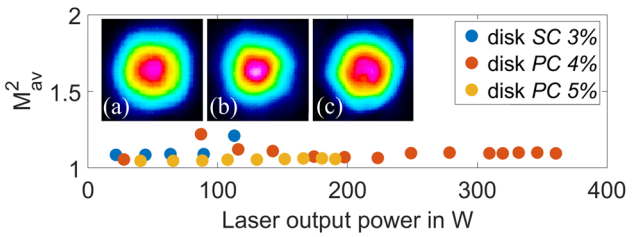

Fig. 11 Beam propagation factor M^2 versus laser output power. The insets show exemplary far-field intensity distributions of the output beams generated using the three laser disks, each at maximum output power

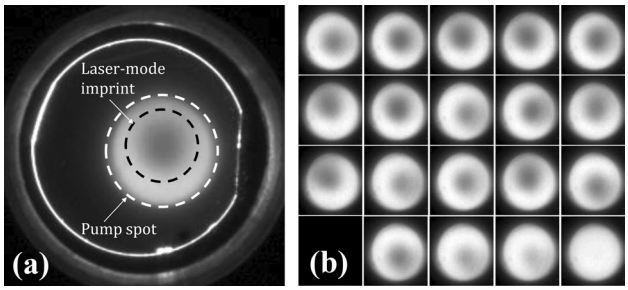

Fig. 12 Photographs of the disk *SC 3%* during fundamental-mode operation: **a** initial alignment. **b** Follow-up images recorded at 1 Hz showing the motion of the mode. The laser operation collapsed in the image on the bottom right, as can be seen due to the lack of the laser-mode imprint

With the the single-crystal disk *SC 3%*, an output power of 113 W, a slope efficiency of 43%, and an optical efficiency of 29.0% were obtained at a $M^2 = 1.2$. In contrast to the ceramic disks, the power achieved with disk *SC 3%* was limited by an unexpected instability of the mode and not by the resonator instability as would be expected due to thermal lensing at higher powers.

It was observed that the position of the laser mode was subject to a lateral oscillation with respect to the pump spot without any changes in the pump power or the alignment of the setup. The higher the pump power, the stronger this effect was, eventually leading to the collapse of the laser operation.

Figure 12a shows a photograph of the aligned state of disk *SC 3%* at its maximum output power in fundamental-mode operation and Fig. 12b shows a sequence of follow-up images recorded at 1 Hz.

It is worth mentioning that the eccentric alignment of the pump spot with respect to the disk was chosen intentionally, as the described effect was the weakest at this position.

It is assumed that this behavior is related to the relatively strong and asymmetric stress-induced birefringence that was observed during the measurement of the depolarization of this disk, but further investigations will be required to clarify this point.

4 Conclusion

In conclusion, it was found that the investigated ceramic and single-crystal Yb:Lu_2O_3 disks exhibit comparable spectroscopic properties, indicating a high purity of the ceramic samples. The lower stress-induced birefringence was found to be a significant advantage of ceramic Yb:Lu_2O_3 disks. In multimode laser operation, all disks delivered kilowatt-class output powers with the highest slope efficiency of 72.1% for the single-crystal and 68.8% for the ceramic disks. Residual scattering losses in the ceramics are suspected to cause this difference. In fundamental-mode laser operation, the ceramics outperformed the single crystal with regard to the output power, potentially due to the lower stress-induced depolarization in the ceramics.

Future work will be dedicated to investigate the suitability of the Yb:Lu_2O_3 ceramics for mode-locked thin-disk lasers.

Author contributions SE performed all measurements and wrote the manuscript. XX, JW and JZ where involved in the fabrication of the ceramics. TG and MAA assisted in the preparation of the manuscript. All authors reviewed the manuscript.

Funding Open Access funding enabled and organized by Projekt DEAL. This study was supported by Deutsche Forschungsgemeinschaft (No. 410806665) and National Natural Science Foundation of China (No. 61861136007).

Declarations

Conflict of interest The authors declare no conflicts of interest.

Open Access This article is licensed under a Creative Commons Attribution 4.0 International License, which permits use, sharing, adaptation, distribution and reproduction in any medium or format, as long as you give appropriate credit to the original author(s) and the source, provide a link to the Creative Commons licence, and indicate if changes were made. The images or other third party material in this article are included in the article's Creative Commons licence, unless indicated otherwise in a credit line to the material. If material is not included in the article's Creative Commons licence and your intended use is not permitted by statutory regulation or exceeds the permitted use, you will need to obtain permission directly from the copyright holder. To view a copy of this licence, visit http://creativecommons.org/licenses/by/4.0/.

References

1. R. Peters, C. Krankel, S. Fredrich-Thornton, K. Beil, K. Petermann, G. Huber, O. Heckl, C. Baer, C. Saraceno, T. Sudmeyer, U. Keller, Appl. Phys. B **102**, 509–514 (2011)
2. K. Petermann, L. Fornasiero, E. Mix, V. Peters, Opt. Mater. **19**(1), 67–71 (2002)
3. V. Petrov, K. Petermann, U. Griebner, V. Peters, J. Liu, M. Rico, P. Klopp, G. Huber. Laser source and system technology for defense and security II **6216**, 62160H. SPIE, (2006)
4. D. Yin, J. Wang, Y. Wang, P. Liu, J. Ma, X. Xu, D. Shen, Z. Dong, L.B. Kong, D. Tang, J. Eur. Ceram. Soc. **40**(2), 444–448 (2020)
5. J. Sanghera, J. Frantz, W. Kim, G. Villalobos, C. Baker, B. Shaw, B. Sadowski, M. Hunt, F. Miklos, A. Lutz, I. Aggarwal, Opt. Lett. **36**(4), 576–578 (2011)
6. S. Esser, C. Rohrer, X. Xu, J. Wang, J. Zhang, T. Graf, M. Abdou Ahmed, Opt. Lett. **46**(24), 6063–6066 (2021)
7. B. Weichelt, K.S. Wentsch, A. Voss, M. Abdou Ahmed, T. Graf, Laser Phys. Lett. **9**(2), 110–115 (2012)
8. R. Peters, C. Krankel, K. Petermann, G. Huber, J. Cryst. Growth **310**(7), 1934–1938 (2008)
9. Z. Liu, G. Toci, A. Pirri, B. Patrizi, Y. Feng, J. Wei, F. Wu, Z. Yang, M. Vannini, J. Li, J. Adv. Ceram. **9**, 674–682 (2020)
10. L.N. Soms, A.A. Tarasov, V.V. Shashkin, Sov. J. Quantum Electron. **10**(3), 350 (1980)
11. J. Dominik, M. Scharun, B. Dannecker, V. Buhner, K. Ertel, D. Bauer, T. Dekorsy, Appl. Opt. **61**(17), 4986–4992 (2022)

12. J.A. Caird, S.A. Payne, P.R. Staber, A.J. Ramponi, L.L. Chase, W.F. Krupke, IEEE J. Quantum Electron. **24**(6), 1077–1099 (1988)
13. I.L. Snetkov, D.E. Silin, O.V. Palashov, E.A. Khazanov, H. Yagi, T. Yanagitani, H. Yoneda, A. Shirakawa, K. Ueda, A.A. Kaminskii, Opt. Express **21**, 21254–21263 (2013)

Publisher's Note Springer Nature remains neutral with regard to jurisdictional claims in published maps and institutional affiliations.